https://doi.org/10.1007/s41230-021-0009-y

Corrosion and chemical behavior of $Mg_{97}Zn_1Y_2$-1wt.%SiC under different corrosion solutions

***Di-qing Wan, Yan-dan Xue, Jia-jun Hu, Hou-bin Wang, Wei Liu**

School of Materials Science and Engineering, East China Jiaotong University, Nanchang 330013, China

Abstract: To explore the corrosion properties of magnesium alloys, the chemical behavior of a high strength $Mg_{97}Zn_1Y_2$-1wt.%SiC alloy in different corrosion environments was studied. Three solutions of 0.2 mol·L^{-1} NaCl, Na_2SO_4 and $NaNO_3$ were selected as corrosion solutions. The microstructures, corrosion rate, corrosion potential, and mechanism were investigated qualitatively and quantitatively by optical microscopy (OM), scanning electron microscopy (SEM), immersion testing experiment, and electrochemical test. Microstructure observation shows that the $Mg_{97}Zn_1Y_2$-1wt.%SiC alloy is composed of α-Mg matrix, LPSO ($Mg_{12}ZnY$) phase and SiC phase. The hydrogen evolution and electrochemical test results reflect that the $Mg_{97}Zn_1Y_2$-1wt.%SiC in 0.2 mol·L^{-1} NaCl solution has the fastest corrosion rate, followed by Na_2SO_4 and $NaNO_3$ solutions, and that the charge-transfer resistance presents the contrary trend and decreases in turn.

Key words: $Mg_{97}Zn_1Y_2$-1wt.%SiC; corrosion rate; corrosion morphology; corrosion mechanism

CLC numbers: TG146.22 **Document code:** A **Article ID:** 1672-6421(2021)01-068-07

1 Introduction

Magnesium alloy is a light engineering material, used in aerospace, automotive and electronics industries due to its high damping capacity, good electromagnetic shielding characteristics, high thermal and electrical conductivity, favorable dimensional stability and machinability [1-3]. Unfortunately, the poor corrosion resistance of Mg alloys is still a key factor restricting its wide application. Therefore, it is vital to prepare the Mg alloys with high strength and corrosion resistance.

Mg-RE-Zn alloys with long-period stacking ordered (LPSO) phase have received considerable attention owing to their unique microstructures and outstanding mechanical properties. It is proved that LPSO phase can significantly improve the strength, ductility, and creep and corrosion resistance of Mg alloy [1, 4-8]. Cheng et al. [9] revealed that Mg-Zn-Y-Ti alloys with rod-like LPSO phases exhibited a more uniform corrosion mode and better corrosion resistance. Wang et al. [10] reported that $Mg_{98.5}Y_1Zn_{0.5}$ alloys containing LPSO phase presented higher corrosion resistance compared with WE43, ZK60 and ZX60 alloys. Nevertheless, research on the corrosion resistance of the Mg-RE-Zn alloy system is still insufficient, especially for the alloy with SiC addition. SiC is often used as the reinforcing phase of magnesium matrix composites due to its low density, high strength and high hardness, good thermal stability, and so on. Research shows that adding an appropriate amount of SiC particles to Mg alloys can enhance the mechanical properties and corrosion resistance [11-13]. Ganguly et al. [13] investigated the effect of SiC_{np} (0.5, 1.0, 2.0, wt.%) addition on corrosion reaction of AZ91-2.0Ca-0.3Sb alloy and reported that all the AZ91-2.0Ca-0.3Sb+$x$$SiC_{np}$ (x=0.5, 1.0, 2.0, wt.%) composites demonstrated a superior corrosion resistance over the matrix alloy. Also, an ultrahigh strength $Mg_{97}Zn_1Y_2$-1wt.%SiC with LPSO phase was successfully prepared by our group [14], and the corrosion resistance of the alloy was further studied in this work.

Normally, gases such as SO_2, O_3, NO_x, HCl and organic acids exist in the atmosphere, and dissolve into the rain to form compounds [15, 16]. Mg alloys exposed to air are corroded due to the presence of anions such as Cl^-, NO_3^- and SO_4^{2-} [17]. Thus, it is necessary to discuss the corrosion of magnesium alloy under those three different anions. Consequently, in this work, the microstructure, corrosion mechanism, and electrochemical behaviors of $Mg_{97}Zn_1Y_2$-1wt.%SiC in 0.2 mol·L^{-1} NaCl, Na_2SO_4 and $NaNO_3$ solutions were characterized and investigated.

***Di-qing Wan**

Male, Professor. His research concerns processing of advanced magnesium alloy. He has published more than 70 papers and one monograph.

E-mail: divadwan@163.com;

Received: 2020-04-22; Accepted: 2020-11-12

2 Experimental procedure

In this experiment, $Mg_{97}Zn_1Y_2$-1wt.%SiC was prepared by high purity Mg (99.99%) and Zn (99.9%), Mg-Y (25wt.%Y) master alloy and SiC particles by conventional casting method. Pure Mg was placed in a crucible preheated to 350 °C and heated to 720 °C in an electric furnace with the heating rate 10 °C·min^{-1}. After holding for 15 min, Mg-Y master alloy, pure Zn and SiC particles were added and kept at 720 °C for another 20 min. The melt was stirred for approximately 3 min when the alloy elements were completely melted, then the molten alloy was poured into the steel mold for air cooling. All samples were cut into 10 mm×10 mm×10 mm cube from prepared $Mg_{97}Zn_1Y_2$-1wt.%SiC.

The corrosion behavior of $Mg_{97}Zn_1Y_2$-1wt.%SiC alloy in 0.2 mol·L^{-1} NaCl solution, Na_2SO_4 solution, and $NaNO_3$ solution was studied by immersion testing. The corrosion rate of the magnesium alloy is obtained by Eq. (1):

$$V_H = V_g / t \quad (1)$$

V_H is the corrosion rate of metal hydrogenation, mL·cm^{-2}·h^{-1}; V_g is the volume of gas collected, mL; and t is corrosion time, h.

The polarization curve and impedance spectrum of magnesium alloys corrosion were studied by electrochemical analysis. The three-electrode system was adopted for the electrochemical test [14], the saturated calomel electrode and platinum electrode were taken as reference electrode and auxiliary electrode, respectively, and the exposed size of samples of 10 mm×10 mm as the working electrode. The test was performed on the electrochemical workstation with a scanning rate of 0.5 mV·s^{-1} for 400 s at the frequency of 1 Hz. The optical microscopy (OM), scanning electron microscopy (SEM) and X-Ray Diffraction (XRD) were used to analyze the microstructure and phase constitution of the samples.

3 Results and discussion

3.1 Microstructure analysis and corrosion rate

Figures 1 and 2 show the microstructure and XRD spectrum of $Mg_{97}Zn_1Y_2$-1wt.%SiC alloy, respectively. The Mg matrix and the secondary phase can be clearly seen from Fig. 1(a). Combining Fig. 1(b) and Fig. 2, the microstructure of $Mg_{97}Zn_1Y_2$-1wt.%SiC alloy is composed of α-Mg, LPSO ($Mg_{12}ZnY$) phase and SiC phase. The LPSO phase is thin strips and distributes at the grain boundaries. Spherical SiC particles are distributed inside the matrix, which could improve the corrosion resistance of the material to a certain extent [13, 19].

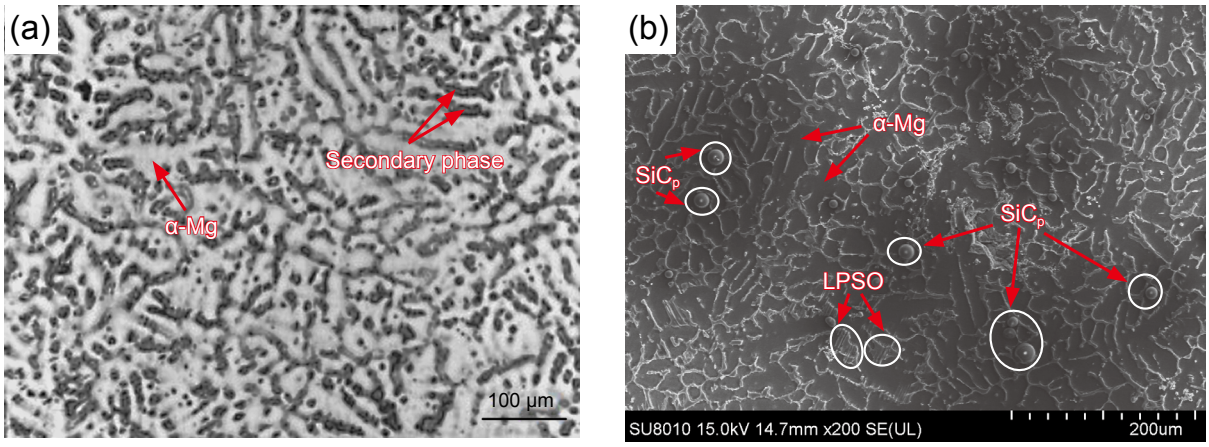

Fig. 1: Microstructure of $Mg_{97}Zn_1Y_2$-1wt.%SiC: (a) OM; (b) SEM

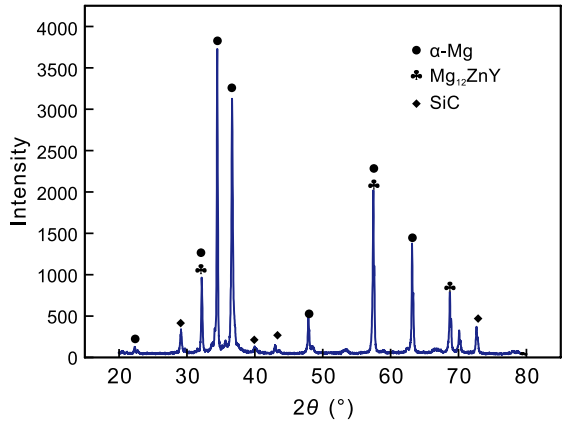

Fig. 2: XRD spectral analysis of $Mg_{97}Zn_1Y_2$-1wt.%SiC

The corrosion rate curves of $Mg_{97}Zn_1Y_2$-1wt.%SiC in different corrosion solutions are shown in Fig. 3. The corrosion rate of the sample in NaCl solution increases rapidly within 1 h to 2 h and then increases slowly. In the Na_2SO_4 solution, the corrosion rate increases in 1 h to 2 h, but then subsequently decreases. In the $NaNO_3$ solution, the corrosion rate of the sample is the slowest, which decreases gradually with time. Therefore, it can be concluded that the corrosion rate of $Mg_{97}Zn_1Y_2$-1wt.%SiC in 0.2 mol·L^{-1} NaCl, Na_2SO_4 and $NaNO_3$ solutions decreases successively.

3.2 Corrosion morphology

Figure 4 shows the SEM morphology of $Mg_{97}Zn_1Y_2$-1wt.%SiC corroded in 0.2 mol·L^{-1} NaCl solution for 1 h to 6 h. As the corrosion time extends, the corrosion products on the sample

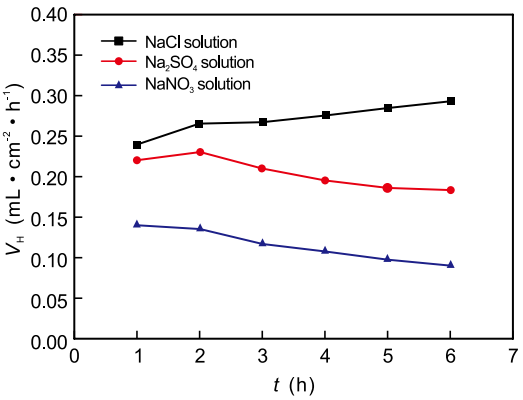

Fig. 3: Corrosion rate curves of $Mg_{97}Zn_1Y_2$-1wt.%SiC in different corrosion solutions

surface increase. It can be seen from Fig. 4(a) that fewer corrosion products are produced on the surface of matrix after the sample was corroded for 1 h. As the corrosion time increases, the degree of corrosion deepens, cracks and holes on the surface increase [Fig. 4(c)], the corrosion products accumulate continuously, become loose and fine [Fig. 4(f)]. The surface of the sample is dominated by pitting corrosion, and the corrosion morphology is granular, loose, and porous, which cannot well block the external solution and protect the matrix.

Figure 5 shows the SEM morphology of $Mg_{97}Zn_1Y_2$-1wt.%SiC corroded in 0.2 mol·L^{-1} Na_2SO_4 solution for 1 h to 6 h. In Fig. 5(a), there are strip-shaped secondary phase and a small amount of flake corrosion product after the sample is corroded for 1 h. In Na_2SO_4 solution, local corrosion occurs preferentially in the region adjacent to the secondary phase, and gradually spreads from the edge of the matrix to the center, which is shown in Figs. 5(b) and (c). From Figs. 5(e) and (f), it can be seen that the corrosion products increase, and cracks deepen. According to Fig. 5, the corrosion product extends and finally covers the whole matrix as the corrosion progresses. However, the corrosion products are not completely spalling

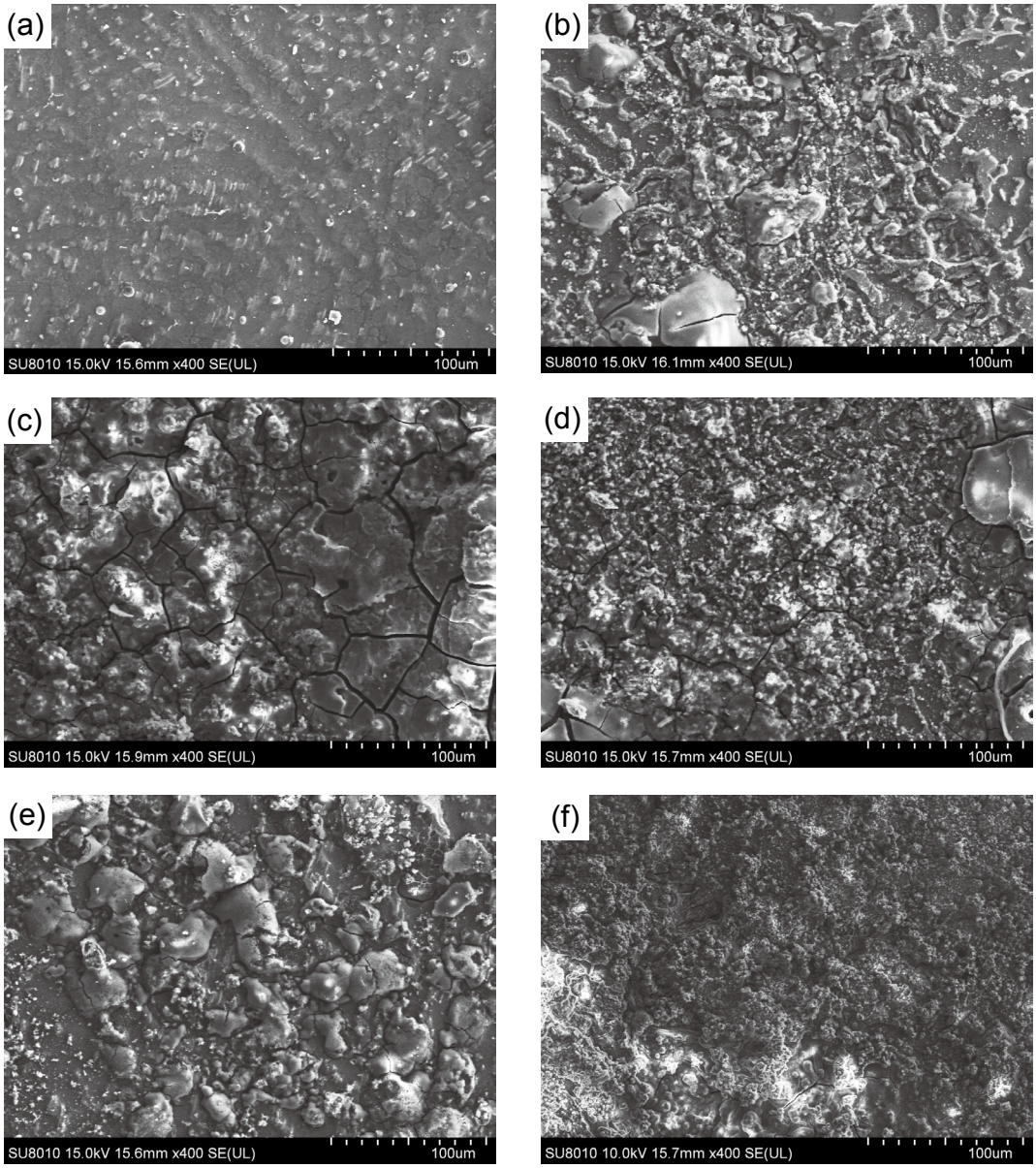

Fig. 4: SEM images of $Mg_{97}Zn_1Y_2$-1wt.%SiC alloys immersed in NaCl solution: (a) 1 h; (b) 2 h; (c) 3 h; (d) 4 h; (e) 5 h; (f) 6 h

after corroding for 6 h, which can provide a good protective barrier for magnesium matrix. By contrast, the corrosion layers of Mg alloys in NaCl solution are completely spalling and the fine particle products remain on the matrix surface. It can be considered that the corrosion ability of SO_4^{2-} is less than Cl^- for the Mg matrix.

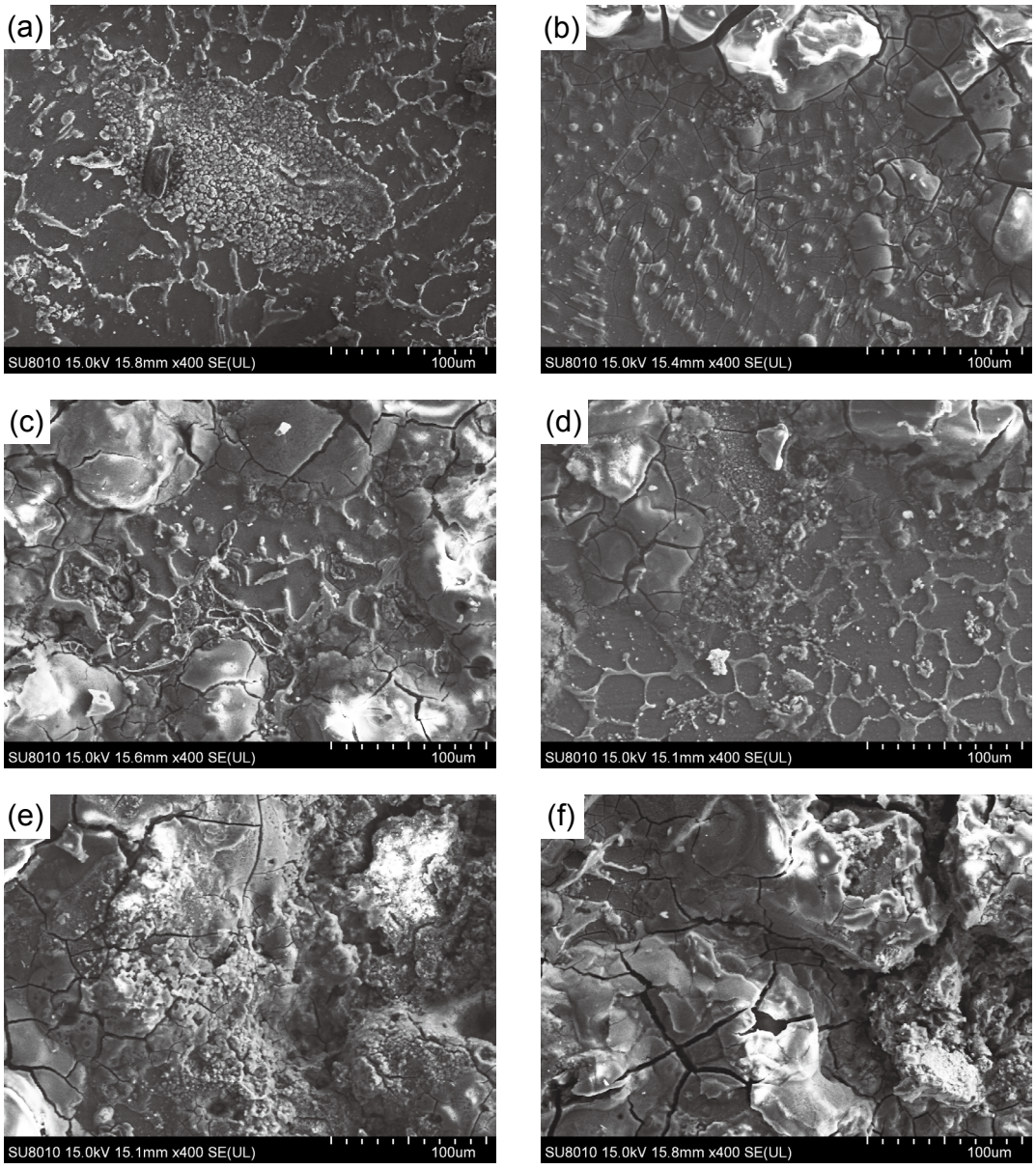

Fig. 5: SEM images of $Mg_{97}Zn_1Y_2$-1wt.%SiC alloys immersed in Na_2SO_4 solution: (a) 1 h; (b) 2 h; (c) 3 h; (d) 4 h; (e) 5 h; (f) 6 h

The SEM morphology of $Mg_{97}Zn_1Y_2$-1wt.%SiC after corrosion in 0.2 mol·L^{-1} $NaNO_3$ solution for 1 h to 6 h is shown in Fig. 6. Like the corrosion behavior in Na_2SO_4 solution, it spreads from the edge of the matrix to the center and eventually covers the entire surface, and the corrosion products increase with corrosion time. In Fig. 6(f), it is found that the corrosion products have deep cracks and etch pits. Different from the corrosion behavior of alloys in NaCl and Na_2SO_4 solutions, the corrosion product of $NaNO_3$ solution does not become granular and isolated, and the corrosion film is not seriously damaged. This indicates that the ability of NO_3^- to penetrate and destroy the corrosion film is weaker than that of Cl^- and SO_4^{2-}, which have weaker corrosion effect on $Mg_{97}Zn_1Y_2$-1wt.%SiC alloys.

The corrosion products on the surface of magnesium alloy are mainly formed by Mg matrix. The more the corrosion products, the more the magnesium matrix consumed, the worse the corrosion resistance. Comparing the corrosion morphology of $Mg_{97}Zn_1Y_2$-1wt.%SiC in three corrosion solutions, it can be found that the surface of the alloy is completely corroded in NaCl solution, there are many cracks and holes in the corrosion products. In Na_2SO_4 and $NaNO_3$ solutions, $Mg_{97}Zn_1Y_2$-1wt.%SiC is partially corroded, while the corrosion products in Na_2SO_4 solution are more and denser than those in $NaNO_3$ solution. Hence, the corrosion resistance of $Mg_{97}Zn_1Y_2$-1wt.%SiC is the worst in NaCl solution, followed by Na_2SO_4 and $NaNO_3$ solutions.

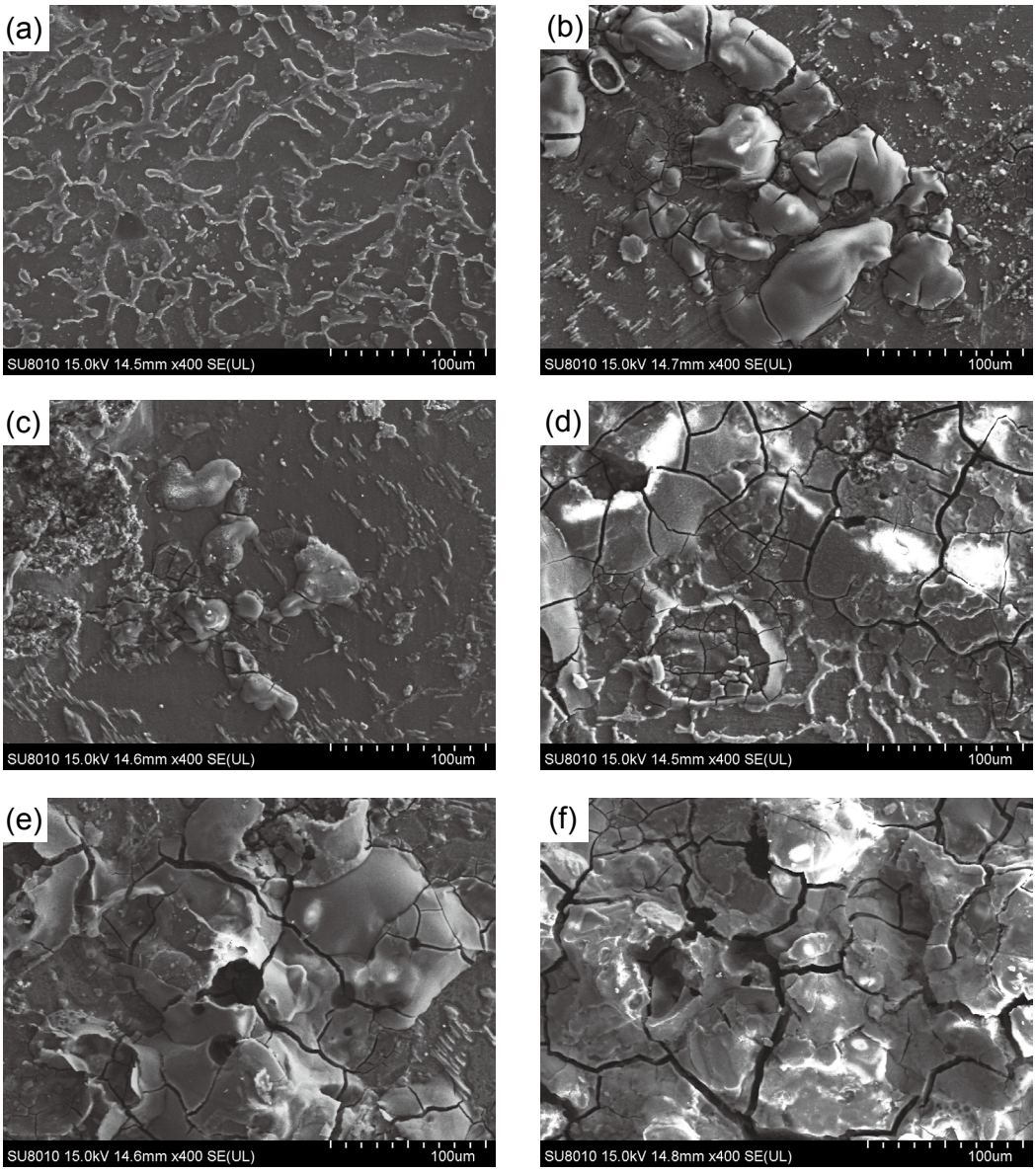

Fig. 6: SEM images of $Mg_{97}Zn_1Y_2$-1wt.%SiC alloys immersed in $NaNO_3$ solution: (a) 1 h; (b) 2 h; (c) 3 h; (d) 4 h; (e) 5 h; (f) 6 h

3.3 Electrochemical testing

As can be seen from the polarization curves of $Mg_{97}Zn_1Y_2$-1wt.%SiC in different corrosion solutions in Fig. 7, the corrosion potential in NaCl and Na_2SO_4 solutions is much more negative than that in $NaNO_3$ solution. Related research shows that negative corrosion potential improves the driving force of corrosion [20], so the corrosion driving force of $Mg_{97}Zn_1Y_2$-1wt.%SiC in NaCl and Na_2SO_4 solutions is greater than that in $NaNO_3$ solution. Moreover, the corrosion driving force of Na_2SO_4 solution is slightly greater than that in NaCl solution. The corrosion current density of $Mg_{97}Zn_1Y_2$-1wt.%SiC in corrosion solutions follows the declining order of NaCl solution > Na_2SO_4 solution > $NaNO_3$ solution, which is consistent with the results of hydrogen evolution measurements.

Figure 8 shows the Nyquist plots of impedance spectrum analysis of $Mg_{97}Zn_1Y_2$-1wt.%SiC in 0.2 mol·L^{-1} NaCl, Na_2SO_4 and $NaNO_3$ solutions. The value of impedance modulus $|Z|$ can reflect the electrode activity and charge-transfer resistance [21-23], and $|Z|$ can be obtained according to $|Z|^2=Z'^2+Z''^2$, where Z' is the real part of the impedance, Z'' is the imaginary part of the impedance. With the increase of the value of impedance

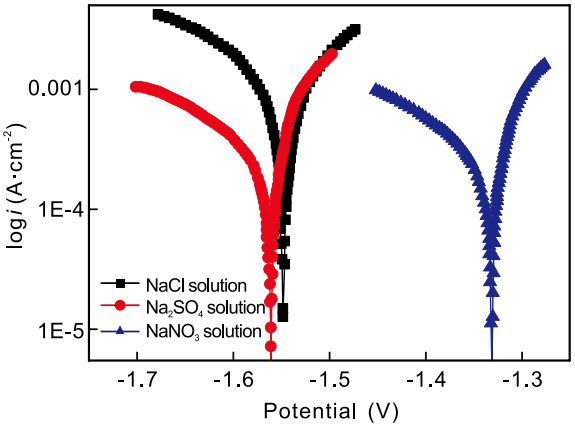

Fig. 7: Polarization curves of $Mg_{97}Zn_1Y_2$-1wt.%SiC in different corrosion solutions

modulus |Z|, the electrode activity decreases, while the charge-transfer resistance increases [24]. It can be seen from Fig. 8 that the arc diameter of NaCl, Na_2SO_4 and $NaNO_3$ solutions increases successively, implying that the activity of $Mg_{97}Zn_1Y_2$-1wt.%SiC decreases sequentially in NaCl, Na_2SO_4 and $NaNO_3$ solutions, and the charge-transfer resistance increases in turn.

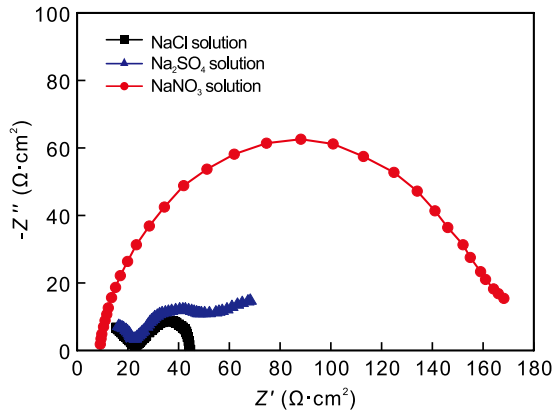

Fig. 8: Nyquist plots of impedance spectra of $Mg_{97}Zn_1Y_2$-1wt.%SiC in different corrosion solutions

3.4 Corrosion mechanism

Generally, the corrosion of magnesium alloys is mainly pitting corrosion [17]. Firstly, pitting occurs selectively on the surface of $Mg_{97}Zn_1Y_2$-1wt.%SiC alloys, and then more etch pits and cracks form on the etched surface. It is found that the corrosion of magnesium alloy in 0.2 mol·L^{-1} NaCl, Na_2SO_4 and $NaNO_3$ solutions always starts from a certain area and spreads to the entire surface. The corrosion product of magnesium is unstable in the corrosion solution, and the active anions are attached to the surface of the magnesium alloy [25, 26]. The corrosion film is damaged by Cl^-, SO_4^{2-} and NO_3^- to form the source of pitting, causing incomplete and uneven thickness of the passivation film on the sample surface.

The anode metal is dissolved along with the growth of corrosion holes on the surface of the Mg alloy. An oxidation reaction (Eq. 2) occurs in the holes, and anions migrate into the holes along with the cations. The magnesium alloy surface undergoes a reduction reaction (Eq. 3), which accelerates the development of corrosion. As the reaction proceeds, the concentration of Mg^{2+} increases and hydrolysis occurs (Eq. 4), which increases the concentration of H^+ in the etched pores and acidifies the solution.

$$Mg \rightarrow Mg^{2+} + 2e^- \quad \text{(anode reaction)} \qquad (2)$$

$$2H_2O + 2e^- \rightarrow H_2 + 2OH^- \quad \text{(cathode reaction)} \qquad (3)$$

$$Mg^{2+} + 2H_2O = Mg(OH)_2 + 2H^+ \quad \text{(hydrolysis reaction)} \qquad (4)$$

In the corrosion solution, the Cl^- continuously invades the corrosion pit and the magnesium matrix is dissolved, resulting in a greater degree of corrosion due to the high conductivity, high adsorption and small apparent size of Cl^- [27]. The corrosion film is damaged by Cl^- to form particles and fall off. However, the SO_4^{2-} and NO_3^- are oxyanions, and the apparent size is larger than Cl^-; they are less liable to penetrate the corrosion film [17], resulting in a weaker and less broken effect on the membrane, so the corrosion degree is weak. As can be seen from Fig. 5(f) and Fig. 6(f), the large cracks are generated on the surface of the matrix in $NaNO_3$ and Na_2SO_4 solutions, and the corrosion products are relatively stable and do not fall off.

The deposition of hydrogen ion and soluble salts greatly increases the conductivity of the film on the metal surface, resulting in higher corrosion currents [28]. In the electrochemical test, the polarization curve of $Mg_{97}Zn_1Y_2$-1wt.%SiC shows the corrosion potential in NaCl and Na_2SO_4 solutions is much lower than in $NaNO_3$ solution. At the same cathode potential, the cathode current density in NaCl solution is higher than that in Na_2SO_4 solution, which indicates that the hydrogen evolution reaction of $Mg_{97}Zn_1Y_2$-1wt.%SiC is more likely to occur in NaCl solution. As the reinforcing phase, SiC can well combine with the matrix interface, refine α-Mg grains and strengthen grain boundaries [29, 30], which improves the corrosion resistance of the alloy to a certain extent.

4 Conclusions

Corrosion and chemical behavior of $Mg_{97}Zn_1Y_2$-1wt.%SiC in 0.2 mol·L^{-1} NaCl, Na_2SO_4 and $NaNO_3$ solutions was studied. The following conclusions can be drawn:

(1) The corrosion rate and degree of $Mg_{97}Zn_1Y_2$-1wt.%SiC are the greatest in NaCl solution, second in Na_2SO_4 solution, and the smallest in $NaNO_3$ solution.

(2) The corrosion current density of $Mg_{97}Zn_1Y_2$-1wt.%SiC increases successively in $NaNO_3$ solution, Na_2SO_4 solution and NaCl solution, while the charge-transfer resistance shows the opposite trend and decreases in turn.

(3) Cl^- has the strongest ability to penetrate and destroy corrosion products and accelerate the corrosion of $Mg_{97}Zn_1Y_2$-1wt.%SiC, while SO_4^{2-} and NO_3^- are relatively weak. The damage of NO_3^-, SO_4^{2-} and Cl^- to the corrosion products increases in order.

Acknowledgements

Financially supported by the National Natural Science Foundation of China (51665012), the Jiangxi Province Science Foundation for Outstanding Scholarship (20171BCB23061, 2018ACB21020), the Primary Research & Development Plan of Jiangxi Province (20192BBEL50019).

References

[1] Shi F, Wang C Q, Zhang Z M. Microstructures, corrosion and mechanical properties of as-cast Mg-Zn-Y-(Gd) alloys. Transactions of Nonferrous Metals Society of China, 2015, 25(7): 2172–2180.

[2] Li Z M, Wan D Q, Huang Y, et al. Characterization of a $Mg_{95.5}Zn_{1.5}Y_3$ alloy both containing W phase and LPSO phase with or without heat treatment. Journal of Magnesium and Alloys, 2017, 5(2): 217–224.

[3] Cabibbo M, Spigarelli S. A TEM quantitative evaluation of strengthening in an Mg-RE alloy reinforced with SiC. Materials Characterization, 2011, 62(10): 959–969.
[4] Zhu J, Chen X H, Wang L, et al. High strength Mg-Zn-Y alloys reinforced synergistically by $Mg_{12}ZnY$ phase and $Mg_3Zn_3Y_2$ particle. Journal of Alloys and Compounds, 2017, 703: 508–516.
[5] Zhang J S, Xu J D, Cheng W L, et al. Corrosion behavior of Mg-Zn-Y alloy with long-period stacking ordered structures. Journal of Materials Science & Technology, 2012, 28(12): 1157–1162.
[6] Zhang X B, Ba Z X, Wang Z Z, et al. Effect of LPSO structure on mechanical properties and corrosion behavior of as-extruded GZ51K magnesium alloy. Materials Letters, 2016, 163: 250–253.
[7] Wan D Q, Wang H B, Li Z M, et al. Aging kinetics of 14H-LPSO precipitates in Mg-Zn-Y alloy. China Foundry, 2020, 17(1): 42–47.
[8] Wan D Q, Hu Y L, Ye S T, et al. Effects of Pb on microstructure, mechanical properties and corrosion resistance of as-cast $Mg_{97}Zn_1Y_2$ alloys. China Foundry, 2018, 15(6): 443–448.
[9] Cheng P, Zhao Y H, Lu R P, et al. Effect of the morphology of long-period stacking ordered phase on mechanical properties and corrosion behavior of cast Mg-Zn-Y-Ti alloy. Journal of Alloys and Compounds, 2018, 764: 226–238.
[10] Wang L S, Jiang J H, Liu H, et al. Microstructure characterization and corrosion behavior of Mg-Y-Zn alloys with different long period stacking ordered structures. Journal of Magnesium and Alloys, 2020, 8(4): 1208–1220.
[11] Esmaily M, Mortazavi N, Svensson J E, et al. On the microstructure and corrosion behavior of AZ91/SiC composites produced by rheocasting. Materials Chemistry & Physics, 2016, 180: 29–37.
[12] Chen H K, Liu J R, Huang W D. Corrosion behavior of silicon nitride bonding silicon carbide in molten magnesium and AZ91 magnesium alloy. Materials Science and Engineering: A, 2006, 415(1–2): 291–296.
[13] Ganguly S, Mondal A K, Sarkar S, et al. Improved corrosion response of squeeze-cast SiC nanoparticles reinforced AZ91-2.0Ca-0.3Sb alloy. Corrosion Science, 2020,166: 108444.
[14] Wang H B. Study on mechanical and damping properties of magnesium-based damping composites with multiple internal friction sources. Nanchang: East China Jiaotong University, 2020. (In Chinese)
[15] Song G, Atrens A. Recent insights into the mechanism of magnesium corrosion and research suggestions. Advanced Engineering Materials, 2007, 9(3): 177–183.
[16] Lindström R, Johansson L G, Svensson J E. The influence of $NaNO_3$ on the atmospheric corrosion of Zinc. Journal of the Electrochemical Society, 2003, 150(12): B583–B588.
[17] Esmaily M, Svensson J E, Fajardo S, et al. Fundamentals and advances in magnesium alloy corrosion. Progress in Materials Science, 2017, 89: 92–193.
[18] Medhashree H, Shetty A N. Electrochemical corrosion study of Mg-Al-Zn-Mn alloy in aqueous ethylene glycol containing chloride ions. Journal of Materials Research & Technology, 2016, 6(1): 40–49.
[19] Loto R T, Babalola P. Corrosion resistance of low SiC particle variation at low weight content on 1060 aluminum matrix composite in sulfate-contaminated seawater. Results in Physics, 2019, 13: 102241.
[20] Liu Y X, Curioni M, Liu Z. Correlation between electrochemical impedance measurements and corrosion rates of Mg-1Ca alloy in simulated body fluid. Electrochimica Acta, 2018, 264: 101–108.
[21] Li Z M. Study on solid solution aging behavior and properties of magnesium alloys with long-period structure. Nanchang: East China Jiaotong University, 2017. (In Chinese)
[22] Ping D H, Hono K, Kawamura Y, et al. Local chemistry of a nanocrystalline high-strength $Mg_{97}Zn_2Y_1$ alloy. Philosophical Magazine Letters, 2002, 82(10): 543–551.
[23] Turhan M C, Weiser M, Jha H, et al. Optimization of electrochemical polymerization parameters of polypyrrole on Mg-Al alloy (AZ91D) electrodes and corrosion performance. Electrochimica Acta, 2011, 56(15): 5347–5354.
[24] Pavlov D, Petkova G. Phenomena that limit the capacity of the positive lead acid battery plates. Journal of the Electrochemical Society, 2002, 149(5): A644–A653.
[25] Zhu Y M, Morton A J, Nie J F. Characterization of intermetallic phases and planar defects in Mg-Zn-Y alloys. Materials Science Forum, 2007, 561: 151–154.
[26] Matsuda M, Li S, Kawamura Y, et al. Variation of long-period stracking order structures in rapidly solidified $Mg_{97}Zn_1Y_2$ alloy. Materials Science and Engineering A, 2005, 393(1–2): 269–274.
[27] Wang X M, Zeng X Q, Zhou Y, et al. Early oxidation behaviors of Mg-Y alloys at high temperature. Journal of Alloys and Compounds, 2008, 460(1–2): 368–374.
[28] Inoue H, Sugahara K, Yamamoto A, et al. Corrosion rate of magnesium and its alloys in buffered chloride solutions. Corrosion Science, 2002, 44(3): 603–610.
[29] Wang X J, Wang N Z, Wang L Y, et al. Processing, microstructure and mechanical properties of micro SiC particles reinforced magnesium matrix composites fabricated by stir casting assisted by ultrasonic treatment processing. Materials & Design, 2014, 57(5): 638–645.
[30] Shen J H, Yin W H, Wei Q M, et al. Effect of ceramic nanoparticle reinforcements on the quasistatic and dynamic mechanical properties of magnesium based metal matrix composites. Journal of Materials Research, 2013, 28(13): 1835–1852.